

Hydrogen Bonding and Proton Transfer to Ruthenium Hydride Complex CpRuH(dppe): Metal and Hydride Dichotomy

Gleb A. Silantyev,[†] Oleg A. Filippov,[†] Peter M. Tolstoy,[‡] Natalia V. Belkova,^{*,†} Lina M. Epstein,[†] Klaus Weisz,[§] and Elena S. Shubina^{*,†}

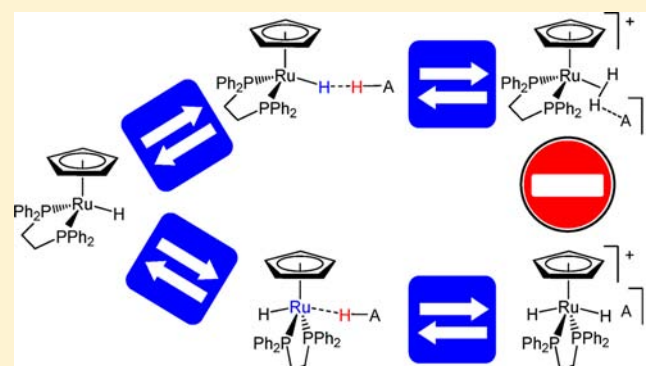
[†]A. N. Nesmeyanov Institute of Organoelement Compounds, Russian Academy of Sciences, Vavilov St. 28, 119991 Moscow, Russia

[‡]Center for Magnetic Resonance, St. Petersburg State University, Universitetskii pr. 26, 198504 Peterhof, Russia

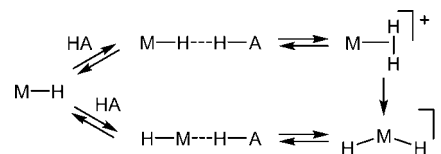
[§]Ernst-Moritz-Arndt-Universität Greifswald, Felix-Hausdorff-Straße 4, 17487 Greifswald, Germany

Supporting Information

ABSTRACT: The combination of variable temperature (190–297 K) IR and NMR spectroscopy studies with quantum-chemical calculations at the DFT/B3PW91 and AIM level had the aim to determine the mechanism of proton transfer to CpRuH(dppe) (**1**, dppe = Ph₂P(CH₂)₂PPh₂) and the structures of intermediates. Dihydrogen bond (DHB) formation was established in the case of interaction with weak proton donors like CF₃CH₂OH. Low-temperature protonation (at about 200 K) by stronger proton donors leads via DHB complex to the cationic nonclassical complex [CpRu(η²-H₂)(dppe)]⁺ (**2**). Thermodynamic parameters of DHB formation (for CF₃CH₂OH: ΔH^o_{HB} = -4.9 ± 0.2 kcal·mol⁻¹, ΔS^o_{HB} = -17.8 ± 0.7 cal·mol⁻¹·K⁻¹) and proton transfer (for (CF₃)₂CHOH: ΔH^o_{PT} = -5.2 ± 0.3 kcal·mol⁻¹, ΔS^o_{PT} = -23 ± 1 cal·mol⁻¹·K⁻¹) were determined. Above 240 K **2** transforms into *trans*-[CpRu(H)₂(dppe)]⁺ (**3**) yielding a mixture of **2** and **3** in 1:2 ratio. Kinetic analysis and activation parameters for the “[Ru(η²-H₂)]⁺ → *trans*-[Ru(H)₂]⁺” transformation indicate reversibility of this process in contrast to irreversible intramolecular isomerization of the Cp* analogue. Calculations show that the driving force of this process is greater stability (by 1.5 kcal·mol⁻¹ in ΔE scale) of the dihydride cation in comparison with the dihydrogen complex. The calculations of the potential energy profile indicate the low barrier for deprotonation of **2** suggesting that the formation of *trans*-[CpRu(H)₂(dppe)]⁺ proceeds via deprotonation of [Ru(η²-H₂)]⁺ to DHB complex, formation of hydrogen bond with Ru atom and subsequent proton transfer to the metal site.



Scheme 1. Two Pathways of Transition-Metal Hydrides Protonation via *syn* and *anti* Hydrogen Bonding



The protonation of the CpRuH(dppe) complex (**1**; dppe = Ph₂P(CH₂)₂PPh₂) by strong acids (HPF₆, (CF₃SO₂)₂C(Ph)D or HBF₄·Et₂O) yields at room temperature the 1:2 mixture of [CpRu(η²-H₂)(dppe)]⁺ (**2**) and *trans*-[CpRu(H)₂(dppe)]⁺ (**3**)^{9,10} whereas the dihydrogen complex **2** is the sole protonation product at 213 K (Scheme 2).¹¹

So, to figure out the reaction mechanism and the possibility of direct proton transfer to the metal atom in the presence of hydride ligand we carried out a variable temperature IR and

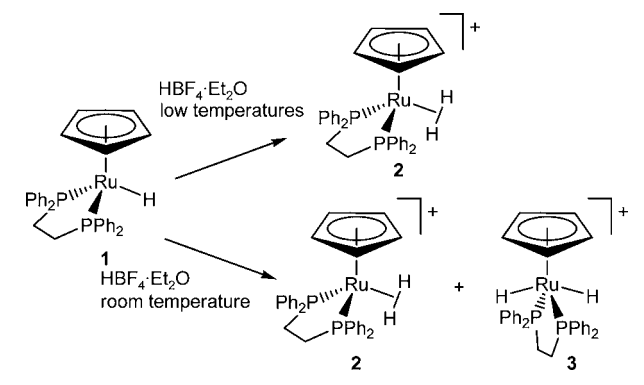
INTRODUCTION

Proton transfer involving transition metal hydrides is an important step of many chemical and biochemical catalytic processes. Protonation of hydrides is known to yield nonclassical η²-H₂ complexes, many of which transform to classical dihydride isomers upon warming. A classical example is the low temperature protonation of the Cp*FeH(dppe) complex described first by Hamon et al.¹ Later we have shown that it proceeds via MH...HA dihydrogen bond formation followed by η²-H₂ → *trans*-dihydride isomerization which occurs as a direct intramolecular rearrangement.^{2–4} The same mechanism has been established for the ruthenium analogue, Cp*RuH(dppe).⁵ At that a number of complexes give a dihydrogen-dihydride mixture as a thermodynamic product of proton transfer.^{6–9} In this case the question arises whether dihydride is formed by simple isomerization of a nonclassical precursor or by deprotonation of the latter with subsequent proton transfer to the metal via a M...HA hydrogen bonded intermediate (Scheme 1).

Received: July 20, 2012

Published: January 25, 2013

Scheme 2. Products of CpRuH(dppe) Protonation by HBF₄·Et₂O at Low and Room Temperatures



NMR spectroscopic study and density functional theory (DFT) calculations of the interaction of **1** with fluorinated alcohols and other proton donors (CF₃CH₂OH (TFE), (CF₃)₂CHOH (HFIP), CF₃COOH (TFA), indole, HBF₄·Et₂O).

EXPERIMENTAL SECTION

Hydride Synthesis. CpRuCl(PPh₃)₂ was synthesized as described¹² and then transformed into CpRuCl(dppe).¹³ The hydride CpRuH(dppe) was obtained by the reaction of CpRuCl(dppe) with sodium methylate in MeOH.¹⁴

Dichloromethane was dried by reflux over CaH₂ and freshly distilled under an argon atmosphere prior to use.

All NMR spectra were measured on Bruker AMX 500 and Bruker AVANCE 600 NMR spectrometers supplied with a specially designed low temperature dual probe-head (SEI, 5 mm tube size, ¹H/¹³C). Eurotherm Variable Temperature Unit was used for temperature stabilization. The temperature was measured with a build-in copper-constantan thermocouple positioned about 1 mm below the bottom of the sample tube. The control unit regulated the heater current to achieve stable temperature using the Zeigler-Nichols PID controller procedure. Stability of the temperature during each experiment was about ±0.2 K.

The IR spectra of CH₂Cl₂ solutions were measured on a Nicolet 6700 FTIR spectrometer in CaF₂ cells (*l* = 2.2 mm). Concentrations of proton donors were 0.006 M for measurements in the ν_{XH} range to avoid self-association.

For the reference measurements the complexes **2** and **3** were prepared in situ by protonation of **1** by 1.2 equiv of HBF₄·Et₂O in CH₂Cl₂ or CD₂Cl₂. Their spectroscopic parameters are in full agreement with those reported in ref 9.

2: ¹H NMR (600 MHz, CD₂Cl₂, 200 K): δ = -9.21 ppm (2H, Ru(η^2 -H₂)); ³¹P{¹H} NMR (212 MHz, CD₂Cl₂, 200 K): δ = 79.3 ppm.

3: ¹H NMR (600 MHz, CD₂Cl₂, 200 K): δ = -8.72 ppm (2H, RuH₂); ³¹P{¹H} NMR (212 MHz, CD₂Cl₂, 200 K): δ = 68.4 ppm; IR (CH₂Cl₂): ν^{as} (RuH₂) = 1984 cm⁻¹, ν^{s} (RuH₂) = 2014 cm⁻¹.

Computational Details. Calculations were performed with the Gaussian09¹⁵ package at the DFT/B3PW91^{16–18} level without any ligand simplification. The basis set for the Ru and P atoms was that associated with the pseudopotential,^{19,20} with a standard double- ζ LANL2DZ contraction,¹⁵ supplemented in the case of P with a set of d-polarization functions.²¹ The carbon and hydrogen atoms of the Cp and dppe ligands together with the atoms of the proton donor molecules (C, F, H) that are not involved in hydrogen bonds were described with a 6-31G basis set.²² The hydridic hydrogen atom and the hydrogen and oxygen atoms of the proton donor molecules involved in hydrogen bonding were described with a 6-31G(d,p) set of basis functions.²³

The structures of the reactants, hydrogen bonded complexes, ion pairs, and transition states were fully optimized with this basis set without any symmetry restrictions. The nature of all of the stationary

points on the potential energy surface was confirmed by vibrational analysis.²⁴ Transition state (TS) structures showed only one negative eigenvalue in their diagonalized force constant matrices, and their associated eigenvectors were confirmed to correspond to the motion along the reaction coordinate under consideration using the intrinsic reaction coordinate (IRC) method.

Natural atomic charges and Wiberg bond indices²⁵ (WBI) were calculated using the natural bond orbital (NBO) analysis²⁶ option as incorporated in Gaussian09. Topological analysis of the electron density distribution function $\rho(r)$ was performed using the AIMALL program package²⁷ based on the wave function obtained by the B3PW91 calculations. AIM extended wave function format allows QTAIM analyses of molecular systems containing heavy atoms described with ECPs. The energy of the hydrogen bonding interaction was estimated using the correlation between the energy of the contact (E_{cont}) and the value of the potential energy density function $V(r)$ in (3, -1) critical point $E_{\text{cont}} = 1/2V(r)$.^{28,29} Hydrogen bond ellipticity, ϵ_{HH} , was defined as $\epsilon = (\lambda_1/\lambda_2 - 1)$, where λ_1 and λ_2 are the negative eigenvalues of the Hessian of the electron density at the bond critical point ordered such that $\lambda_1 < \lambda_2 < 0$.

RESULTS AND DISCUSSION

Interaction with Weak Proton Donors: Hydrogen Bonding.

Formation of a hydrogen bond between **1** and weak proton donors such as indole and TFE at low temperatures in dichloromethane was established by IR spectroscopy. In the presence of excess **1** the intensity of the $\nu_{\text{XH}}^{\text{free}}$ bands of the proton donors decreases, and new wide $\nu_{\text{XH}}^{\text{bonded}}$ bands appear at lower frequencies. The band shift, $\Delta\nu_{\text{XH}} = \nu_{\text{XH}}^{\text{free}} - \nu_{\text{XH}}^{\text{bonded}}$, increases from indole to TFE being 223 and 266 cm⁻¹, respectively. These data allow estimating the enthalpy of hydrogen bond formation $\Delta H_{\text{HB}}^{\circ} = -4.3$ and -4.9 kcal·mol⁻¹ for complexes of **1** with indole and TFE, respectively. The value obtained for **1**·TFE is in good agreement with that obtained from the temperature dependence of **1**·TFE hydrogen bond formation constants $\Delta H_{\text{HB}}^{\circ} = -4.9 \pm 0.2$ kcal·mol⁻¹; $\Delta S_{\text{HB}}^{\circ} = -17.8 \pm 0.7$ cal·mol⁻¹·K⁻¹. The complex basicity in hydrogen bonding,^{30–32} $E_j = \Delta H_{\text{HB}}^{\circ}/(P_i \Delta H_{11}^{\circ})$ or $E_j = \Delta H_{\text{HB}}^{\circ}/P_i/\Delta H_{11}^{\circ} = 1.21$, is lower than that of Cp*RuH(dppe) ($E_j = 1.39^5$) and higher than that of CpRuH(CO)(PCy₃) ($E_j = 1.02$).³³

The IR spectrum of **1** in the range of M-H stretching vibrations features a wide ($\Delta\nu_{1/2} = 67$ cm⁻¹) band at 1937 cm⁻¹, which is asymmetric because of the overlap with dppe ligand vibrations (overtone of the phenyl rings). In the presence of increasing amount of TFE the ν_{RuH} band intensity increases by 11–23% whereas its maximum shifts to lower frequencies (Figure 1). Band deconvolution shows the presence of a new $\nu_{\text{MH}}^{\text{bonded}}$ band at 1928 cm⁻¹ (Figure 1). These changes indicate the interaction of the proton donor with the hydride ligand, that is, formation of a dihydrogen bond (DHB) (**1'**).^{34,35}

The DHB formation was confirmed by NMR spectra under similar conditions. The hydride triplet in ¹H NMR shifts from $\delta_{\text{RuH}} -14.12$ ppm for **1** to -14.30 in the presence of 7 equiv of TFE at 200 K in CD₂Cl₂ (Figure 2) whereas the ³¹P{¹H} resonance shifts from 90.3 ppm to 89.4 ppm. Such changes are typical of dihydrogen bond formation^{32,36,37} resulting from the fast equilibrium between the complex **1'** and free hydride **1**. The minimum of the longitudinal relaxation time of the hydride resonance $T_{1 \text{ min}}$ decreases from 1050 ms (210 K, 500 MHz) to 647 ms (210 K, 500 MHz) in the presence of 4 equiv of TFE. That allowed estimating the H···H distance $d_{\text{HH}} = 1.96$ Å in the dihydrogen bonded complex taking into account the

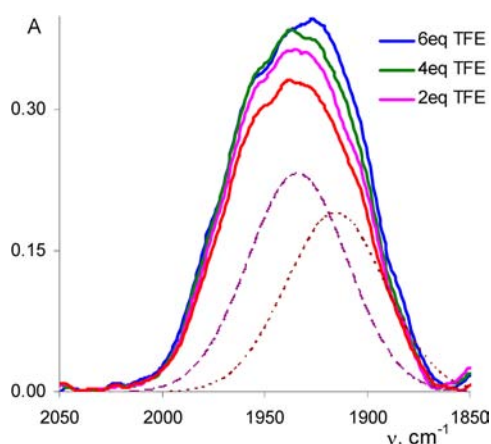


Figure 1. IR spectra (ν_{MH} region) of CpRuH(dppe) (**1**, 0.025 M; red line) and **1** in the presence of 2, 4, and 6 equiv of TFE. CH_2Cl_2 , 200 K, $l = 2.2$ mm. Deconvolution of the blue line: $\nu_{\text{MH}}^{\text{free}}$ (dashed) and $\nu_{\text{MH}}^{\text{bonded}}$ (dotted).

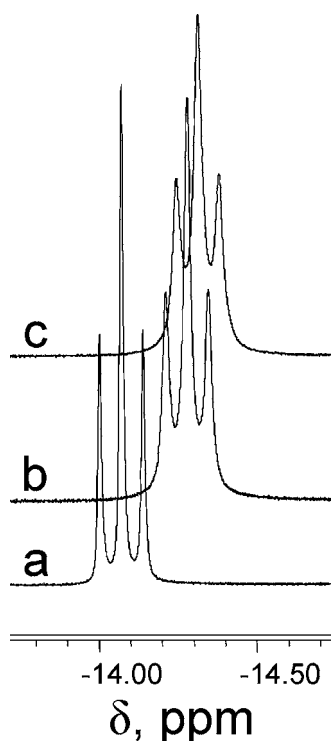


Figure 2. ^1H NMR spectra (hydride region, 500 MHz) of CpRuH(dppe) in the presence of TFE: 0 (a), 4 (b), and 7 (c) equiv. CD_2Cl_2 , 200 K.

equilibrium constants obtained from the IR data.^{36,38} Similarly in the presence of 6 equiv of HFIP the $T_{1\text{min}}$ of hydride resonance decreases from 1383 ms (190 K, 600 MHz) to 487 ms (195 K, 600 MHz) yielding the H \cdots H distance in the DHB complex $d_{\text{HH}} = 1.91$ Å.

Interaction with Stronger Proton Donors: Proton Transfer Equilibrium. Interaction of **1** with 7 equiv of HFIP at 195 K in CD_2Cl_2 leads to partial proton transfer with the formation of dihydrogen complex **2** which is characterized by the hydride resonance at -9.21 ppm (Figure 3, the insignificant amount of dihydride **3** is observed at -8.72 ppm probably because of the local warming of the sample). On the basis of the data reported for other hydride complexes,³⁹ one

can safely assume that **2** (and **3**) exists as contact ion pairs stabilized by a hydrogen bond between the cation and anion (Scheme 3).

With the temperature increase the proton transfer equilibrium shifts toward free (**1**) and dihydrogen-bonded (**1'**) hydride (Scheme 3) as is evident from the redistribution of the signals intensities (Figure 3, Supporting Information, Figure S1). Integration of signals in the temperature range 195–225 K allowed estimating the proton transfer equilibrium constants K_{PT} . The analysis of their temperature dependence (Supporting Information, Figure S1) gave the thermodynamic parameters of the proton transfer step: $\Delta H_{\text{PT}}^{\circ} = -5.2 \pm 0.3$ kcal \cdot mol $^{-1}$ and $\Delta S_{\text{PT}}^{\circ} = -23 \pm 1$ cal \cdot mol $^{-1}\cdot$ K $^{-1}$. These values are in accord with those reported for proton transfer to various hydride complexes^{37,39} when the negative entropy change reflects the more organized solvent structure around the hydrogen bonded ion pair.

To get more information on dynamic exchange processes, a two-dimensional ^1H - ^1H EXSY experiment was carried out for a solution of **1** in CD_2Cl_2 in the presence of 10 equiv of HFIP at 235 K. As shown by the cross-peak in Figure 4, the hydrogen exchange occurs between **2** and the neutral forms **1/1'** in line with the proton transfer mechanism proposed above (Scheme 3).

Further information about the structure of the hydrogen bonded complex and the proton transfer product was obtained from the study of the interaction of **1** with CF_3COOH by IR and NMR spectroscopies. Interestingly, the interaction of **1** with this acid at 200 K leads to partial proton transfer and formation of both **2** and **3**. Addition of 0.5 to 1.5 equiv of CF_3COOH to a 0.025 M solution of **1** in CH_2Cl_2 causes a decrease of the $\nu_{\text{RuH}}(\mathbf{1})$ band intensity and the appearance of $\nu_{\text{RuH}}(\mathbf{3})$ bands at 2014 and 1989 cm^{-1} assigned to $\nu_{\text{RuH}_2^s}$ and $\nu_{\text{RuH}_2^{\text{as}}}$, respectively (Figure 5).³⁵ Full proton transfer is observed in the presence of over 2 equiv of acid as confirmed by ^1H NMR spectra according to which both **2** and **3** are present in solution in the ratio 2:1 as determined by integration of the corresponding high-field resonances. This ratio is independent of the acid excess and does not change up to 240 K. Above this temperature the 2:3 ratio increases reaching the equilibrium value of 1:2 at 298 K similar to that reported for the BF_4 counteranion.¹⁰ These changes correspond to the free energy (ΔG) values of -0.4 (at 298 K) and -0.3 (at 200 K) kcal \cdot mol $^{-1}$ for $\mathbf{2} \rightleftharpoons \mathbf{3}$ equilibrium, and a van't Hoff plot gives $\Delta H = -1.8 \pm 0.1$ kcal \cdot mol $^{-1}$, $\Delta S = -5.7 \pm 0.4$ cal \cdot mol $^{-1}\cdot$ K $^{-1}$.

IR spectra of **1/CF₃COOH** mixture (0.5 equiv of acid) in the range of $\nu_{\text{CO}}(\text{CF}_3\text{COOH})$ and $\nu^{\text{as}}_{\text{OCO}}(\text{CF}_3\text{COO}^-)$ show the appearance of the $\nu^{\text{as}}_{\text{OCO}}$ band of the anion at 1685 cm^{-1} as expected for partial proton transfer (Scheme 4). The less intense bands at 1782 and 1735 cm^{-1} belong to the ν_{CO} vibrations of the acid in the hydrogen bonded complex of **1** with two CF_3COOH molecules (Scheme 4a).⁴⁰ These three bands increase upon further addition of the acid (Supporting Information, Figure S2) in agreement with the right shift of hydrogen bonding and proton transfer equilibrium (Scheme 4b). At 2.5-fold acid excess the additional band appears in the spectrum at 1645 cm^{-1} belonging to $\nu^{\text{as}}_{\text{OCO}}$ vibrations of homoconjugated anion $[\text{CF}_3\text{COO}(\text{CF}_3\text{COOH})_n]^-$. This indicates dissociation of hydrogen bonded ion pair in the presence of excess acid.⁴⁰

Proton Transfer and Formation of *trans*-Dihydride. As mentioned above, when fluorinated alcohols are used as proton donors the dihydrogen complex **2** is the only proton transfer

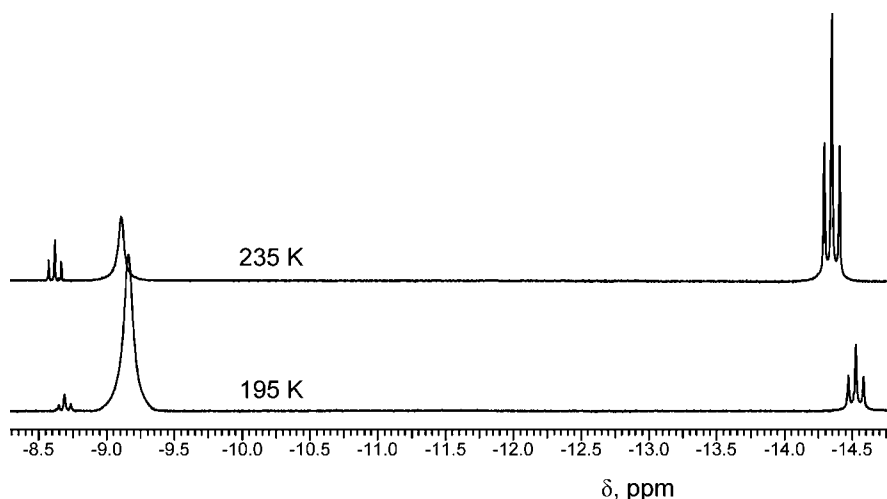
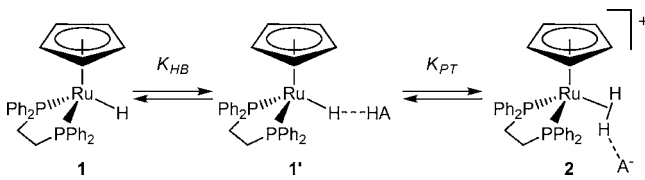


Figure 3. ^1H NMR spectra of **1** (hydride region, 600 MHz) in the presence of 7 equiv of HFIP. 195 and 235 K, CD_2Cl_2 .

Scheme 3. Mechanism of Proton Transfer to CpRuH(dppe) (1**) via Dihydrogen Bonded Complex (**1'**) Formation**



product below 240 K. The temperature increase shifts proton transfer equilibrium to the left, toward the DHB complex **1'** and starting hydride **1** (Figure 3). Formation of the *trans*-

dihydride **3** begins above 240 K. When 10 equiv of HFIP were used at low temperature (190 K) in CD_2Cl_2 the formation of the dihydrogen complex **2** was quantitative (only traces of **3** were observed, Figure 6). With the temperature increase to 210 K (with 5 K step) a slight change in the **2** to **3** intensity ratio was observed in favor of the latter. At 215 K a triplet at -14.66 ppm appears in the spectrum that belongs to the averaged signal of the hydride ligand in free (**1**) and hydrogen-bonded (**1'**) complexes. The position of this signal is determined by the position of the dihydrogen bond formation equilibrium, shifting upfield at higher content of **1'**. Analysis of the data acquired at different temperatures showed that the temperature increase

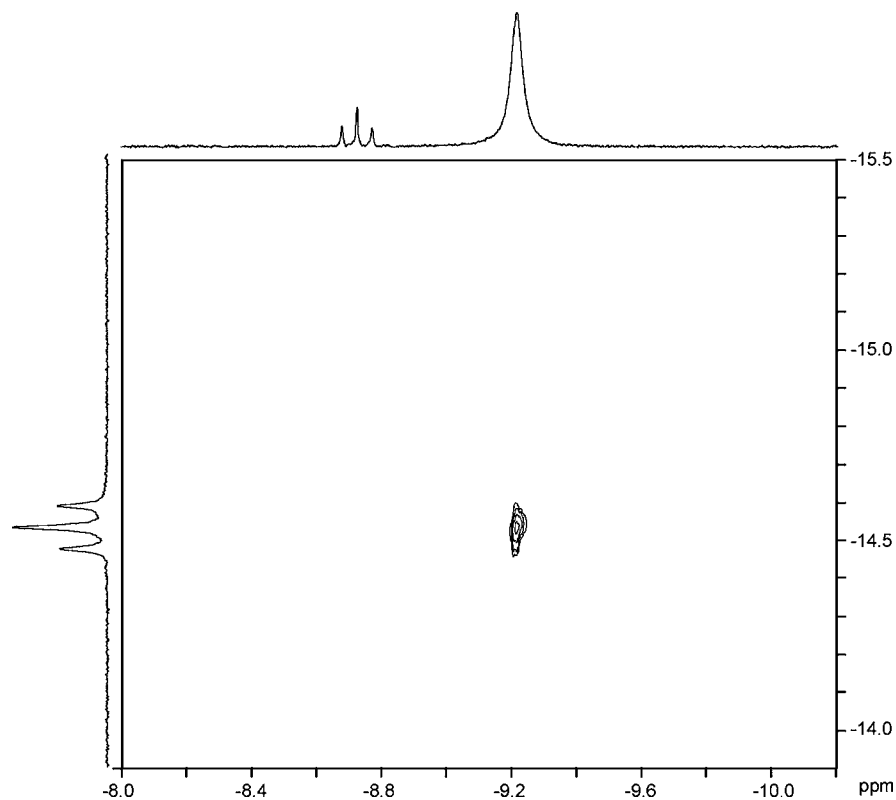


Figure 4. 2D EXSY spectrum of **1** in the presence of 10 equiv of HFIP in CD_2Cl_2 at 235 K (100 ms mixing time). Corresponding 1D spectral regions are shown at the top and to the left.

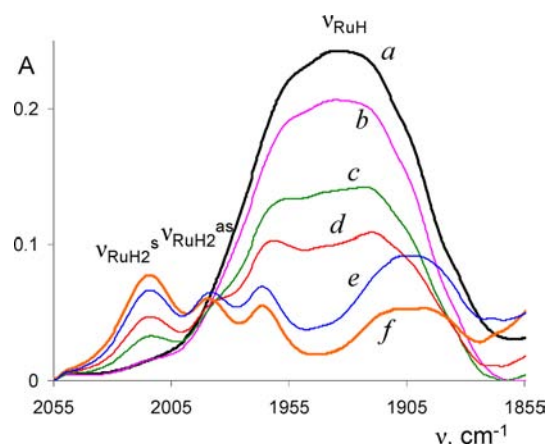


Figure 5. IR spectra (ν_{MH} region) of CpRuH(dppe) (**1**, 0.025 M) and **1** in the presence of increasing amount of TFA: 0 (*a*), 0.5 (*b*), 1 (*c*), 1.5 (*d*), 2 (*e*), 2.5 (*f*) equiv. The intensity increase on going from spectrum *e* to *f* is due to the impact of ν_{CO} absorption of the acid ($\nu_{\text{CO}} = 1800 \text{ cm}^{-1}$). CH_2Cl_2 , 200 K, $l = 1.2 \text{ mm}$.

shifts the equilibrium between **1** and **1'** to the left; that is manifested by the decrease of $\Delta\delta = \delta_1 - \delta_{(1+\text{ROH})}$ values (Supporting Information, Table S1).

The mole fractions of the species in the equilibrium (Supporting Information, Table S1) were calculated in the temperature range 215–265 K from the data obtained by integration of the corresponding signals (Figure 6). Changes of mole fractions with temperature are plotted in Figure 7, showing that the decrease of the concentration of **2** is accompanied by the formation of the neutral forms (due to the deprotonation of **2**) and of *trans*-dihydride **3**. However, the concentration of **3** practically does not increase above 255 K and decreases above 260 K pointing to the reversible formation of *trans*-dihydride due to the left-hand shift of the protonation equilibrium leading to the steady growth of the neutral forms.

At 265 K the predominant species in the presence of 10 equiv of HFIP in CD_2Cl_2 is **1/1'** (74.1%). The small amount of dihydride **3** formed under these conditions does not change when the temperature is decreased to 200 K (Supporting Information, Figure S3) whereas the resonance of **2** appears at 250 K and grows with cooling. This confirms the reversibility of the formation of the cationic complexes **2** and **3** and the kinetic preference of the hydride protonation.

Thus, the dihydrogen bonded complex **1'** is the intermediate of the proton transfer yielding the nonclassical complex **2**. Formation of **2** is reversible as evidenced by the increase of its resonance upon cooling accompanied by disappearance of the

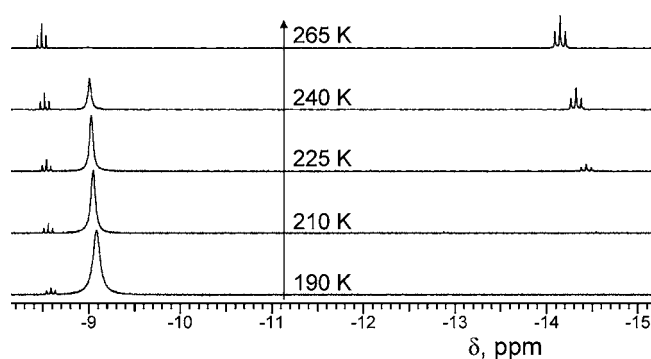


Figure 6. ^1H NMR spectra (hydride region, 600 MHz) of CpRuH(dppe) (**1**) in the presence of 10 equiv of HFIP at different temperatures, CD_2Cl_2 .

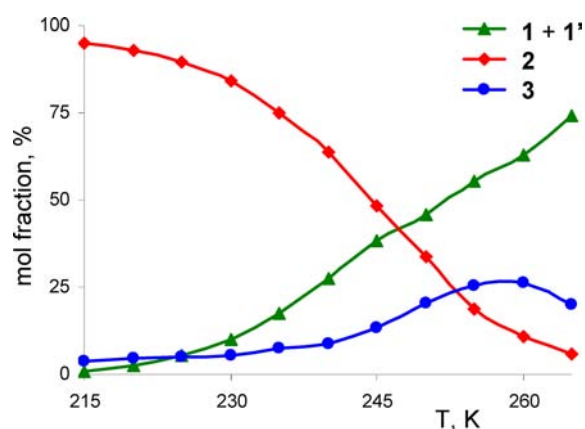
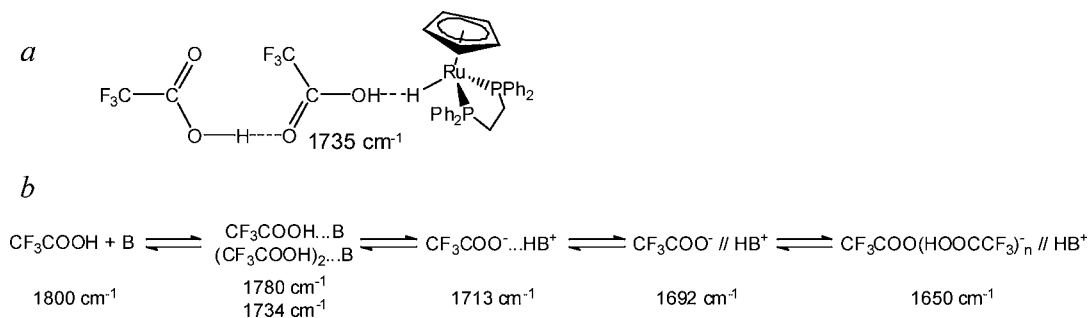


Figure 7. Temperature dependence of the mol fraction of the molecular (**1 + 1'**) and ionic (**2** and **3**) species formed at **1**/HFIP ratio 1:10.

neutral forms (**1 + 1'**) signal. However the data described so far do not allow to discriminate whether **3** is formed by direct isomerization of **2** (as for its Cp* analogue⁴) or by deprotonation-reprotonation pathway via *anti* hydrogen bond to the metal. To address this point we studied the reaction kinetics and performed DFT calculations (see below).

Transformation of **2** to **3** takes time at low temperatures. The kinetics of this transformation was studied by ^1H NMR monitoring of corresponding hydride resonances at 250–265 K (Figure 8a). Complex **2** was generated by in situ protonation of **1** with HFIP or HBF_4 at a temperature of about 200 K, when proton transfer quantitatively gives a $\eta^2\text{-H}_2$ complex. Kinetic curves of isomerization were obtained from integration of **2** and

Scheme 4. (a) Hydrogen Bonded Complex $1 \cdot (\text{TFA})_2$. (b) Equilibria between Molecular and Ionic Forms of CF_3COOH and Corresponding ν_{CO} or ν_{OCO} Vibration Frequencies



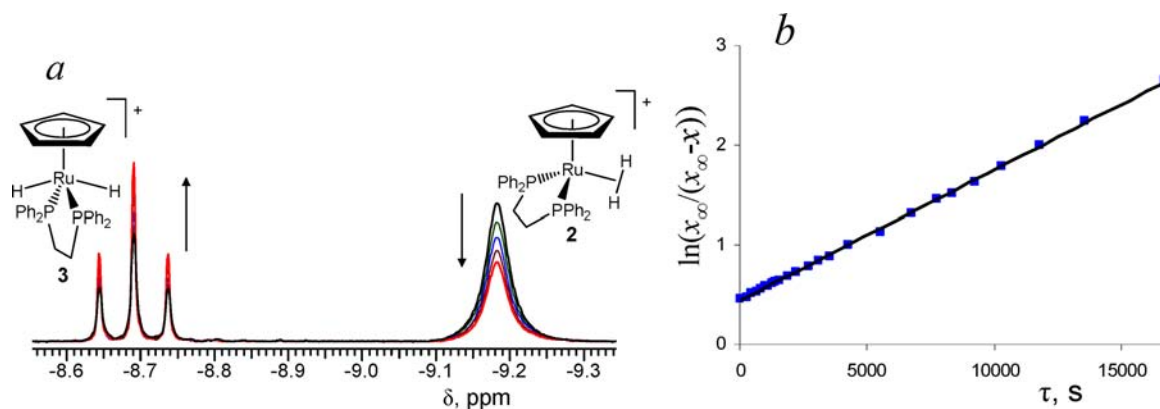


Figure 8. ^1H NMR monitoring of the 2 to 3 transformation (left) and corresponding kinetic plot linearized in the coordinates of reversible first-order reaction (right). 250 K, CD_2Cl_2 .

Table 1. Isomerization Equilibrium Constant K_{isom} , Rate Constants of Direct (k_1) and Reverse (k_2) Reactions, the Reaction Free Energy (ΔG_{isom}), and the Activation Free Energy (ΔG^\ddagger) for the 2 to 3 Transformation

HA	T , K	K_{isom}	$10^4 k_1$, s^{-1}	$10^4 k_2$, s^{-1}	ΔG_{isom} , $\text{kcal}\cdot\text{mol}^{-1}$	ΔG^\ddagger , $\text{kcal}\cdot\text{mol}^{-1}$
HFIP	246	2.12	0.49 ± 0.01	0.23 ± 0.01	-0.37	19.14
	250	1.98	0.86 ± 0.02	0.43 ± 0.02	-0.34	19.21
	253	1.91	1.5 ± 0.02	0.78 ± 0.02	-0.33	19.18
	258	1.92	2.4 ± 0.02	1.3 ± 0.02	-0.33	19.32
HBF ₄	253	1.85	1.2 ± 0.02	0.65 ± 0.02	-0.31	19.3
	260	2.07	3.1 ± 0.03	1.5 ± 0.03	-0.37	19.3

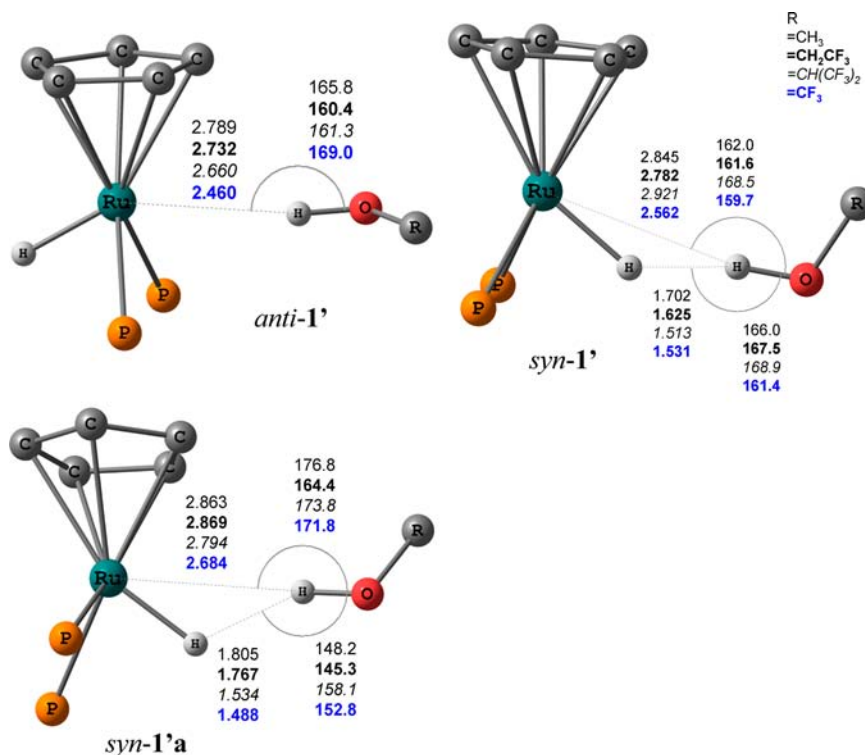


Figure 9. Computed structural parameters of the hydrogen bonded complexes between $\text{CpRuH}(\text{dppe})$ and CH_3OH , $\text{CF}_3\text{CH}_2\text{OH}$ (bold), $(\text{CF}_3)_2\text{CHOH}$ (italic), and CF_3OH (bold, blue).

3 signals at different reaction times τ . Interestingly, kinetic plots become linear in $\ln(x_\infty/(x_\infty - x))$ coordinates (Figure 8b), where x is the amount of nonreacted complex 2 (or the amount of complex 3 formed) at time τ , x_∞ is the amount of 2 at equilibrium. The slope of this line is $k_1 + k_2$ and together with $K_{\text{isom}} = k_1/k_2 = [3]/[2]$ gives direct (k_1) and reverse (k_2) rate

constants of complex 3 formation. Such rate law corresponds to a reversible first-order reaction of the isomerization of $[\text{CpRu}(\eta^2\text{-H}_2)(\text{dppe})]^+$ (2) into $[\text{CpRu}(\text{H})_2(\text{dppe})]^+$ (3) in contrast to irreversible isomerization of $[\text{Cp}^*\text{Ru}(\eta^2\text{-H}_2)(\text{dppe})]^+$ to $[\text{Cp}^*\text{Ru}(\text{H})_2(\text{dppe})]^+$.⁵

The temperature range from 240 to 260 K turned to be the most convenient for NMR monitoring of the isomerization process. The values of the equilibrium constant K_{isom} , the rate constants of direct (k_1) and reverse (k_2) reactions obtained in the presence of 20 equiv of HFIP are gathered in Table 1 together with the free energies ΔG_{isom} and ΔG^\ddagger calculated from these data.

Analysis of the temperature dependence of the rate constant for direct reaction k_1 gives activation enthalpy (ΔH^\ddagger) and entropy (ΔS^\ddagger) of $16 \pm 1 \text{ kcal}\cdot\text{mol}^{-1}$ and $-13 \pm 5 \text{ cal}\cdot\text{mol}^{-1}\cdot\text{K}^{-1}$, respectively. These numbers are very similar to $\Delta H^\ddagger = 17.6 \pm 0.9 \text{ kcal}\cdot\text{mol}^{-1}$ and $\Delta S^\ddagger = -7.8 \pm 0.6 \text{ cal}\cdot\text{mol}^{-1}\cdot\text{K}^{-1}$ reported for the closely related $[\text{CpRuH}_2(\text{dmdppe})]^+$.⁶ The negative activation entropy indicates an ordered (associative) transition state typical for proton transfer reactions⁴¹ and is in contrast with positive values found for isomerization of $[\text{Cp}^*\text{M}(\eta^2\text{-H}_2)(\text{dppe})]^+$.^{4,5,42}

Kinetics of the transformation of **2** into **3** was also studied in the presence of higher HFIP excess (30 equiv) at 258 K. The values of rate constants for direct (k_1) and reverse (k_2) reactions are practically the same as in the presence of 20 equiv of HFIP giving the same values of free energies (compare to Table 1): $k_1 = 2.4 \times 10^{-4} \text{ s}^{-1}$, $k_2 = 1.2 \times 10^{-4} \text{ s}^{-1}$, $\Delta G^\ddagger = 19.33 \text{ kcal}\cdot\text{mol}^{-1}$, and $\Delta G_{\text{isom}} = -0.34 \text{ kcal}\cdot\text{mol}^{-1}$. When tetrafluoroboric acid (1.1–1.5 equiv) was used to generate **2** the rate constants of direct (k_1) and reverse (k_2) reaction showed rather small difference from those obtained in the presence of HFIP at the same temperature (Table 1), not allowing the solid conclusion about the counterion effect on the $\mathbf{2} \rightleftharpoons \mathbf{3}$ transformation rate. But the kinetic data obtained do allow suggesting that transformation of the dihydrogen **2** to the dihydride **3** is reversible for any strong acid.

Computational Study: Hydrogen Bonding. In the case of half-sandwich cyclopentadienyl Group 8 metal hydride complexes of type $(\text{C}_5\text{R}_5)\text{MHL}_2$ ($L_2 = 2 \text{ PR}_3$ or bidentate diphosphine) a proton donor attack on the hydride ligand side (*syn*) would lead to a DHB complex and $\eta^2\text{-H}_2$ proton transfer products, whereas the attack at the opposite side (*anti*) would result in $\text{M}\cdots\text{HA}$ hydrogen bonding and *trans* dihydride formation as the result of proton transfer.

The computational analysis of hydrogen bonding and proton transfer was carried out for the real complex $\text{CpRuH}(\text{dppe})$ at the DFT/B3PW91 level to allow comparison with the data reported for the $\text{Cp}^*\text{RuH}(\text{dppe})$ complex.⁵ The two expected minima (*syn-1'* and *anti-1'*) were indeed found (Figure 9). Surprisingly, another minimum was found for hydrogen bonded adducts with alcohol being at the hydride side (*syn-1'a*, Figure 9), which differs by the orientation of the alkyl substituent of the alcohol and the parameters of the $\text{MH}\cdots\text{HO}$ moiety. The formation energies of all adducts are gathered in Table 2. The details of the electron density analysis and AIM analysis are given in Supporting Information, Tables S2 and S3.

Inspection of the data in Figure 9 shows that both *syn-1'* and *syn-1'a* complexes can be described as bifurcate adducts with simultaneous interaction of the ROH proton with the hydride hydrogen and the metal. Detailed analysis of such bifurcate hydrogen bonds was recently described by some of us for $\text{Cp}^*\text{MH}(\text{dppe})$ complexes.⁴³ The major difference between the two structures *syn-1'* and *syn-1'a* is in the O–H \cdots M and O–H \cdots H angles, the latter being more acute in *syn-1'a*. At that the (O)H \cdots H distance is longer in *syn-1'a* than in *syn-1'*, whereas (O)H \cdots M distance is shorter. Notably, “Atoms in molecule” (AIM) analysis^{44–46} showed just one bond critical point (3,

Table 2. Interaction Energies (in kcal·mol⁻¹) Relative to the Isolated Reactants

ROH	adduct	ΔE	ΔE_{ZPVE}	E_{cont}^a
CH ₃ OH	<i>syn-1'</i>	-6.3	-5.3	-4.2
	<i>syn-1'a</i>	-4.9	-3.8	-3.4
	<i>anti-1'</i>	-1.7	-0.5	-2.0
CF ₃ CH ₂ OH	<i>syn-1'</i>	-7.4	-6.9	-4.9
	<i>syn-1'a</i>	-6.7	-6.3	-3.6
	<i>anti-1'</i>	-5.0	-4.1	-2.2
(CF ₃) ₂ CHOH	<i>syn-1'</i>	-8.0	-7.6	-6.1
	<i>syn-1'a</i>	-10.1	-9.4	-6.1
	<i>anti-1'</i>	-6.2	-5.4	-2.4
CF ₃ OH	<i>syn-1'</i>	-12.2	-11.8	-6.2
	<i>syn-1'a</i>	-12.0	-11.5	-6.8
	<i>anti-1'</i>	-7.6	-7.2	-3.8

^aThe values determined from the AIM analysis data.

–1) in either complex that binds two hydrogens (Supporting Information, Figure S4, Table S2). The (O)H \cdots H interaction is predominant in both complexes independent of ROH: delocalization indices (DI)^{43,47} are always higher for the (O)H \cdots H contacts than for the (O)H \cdots M ones (Supporting Information, Table S2). However, the deviation of the bond path from linearity is evident from higher ellipticity values for *syn-1'a* complexes. Thus, both geometrical and electronic parameters indicate that *syn-1'* and *syn-1'a* are DHB complexes with higher metal involvement in *syn-1'* complexes.

Inspection of the hydrogen bonding energies reveals interesting trends. The *syn-1'* structure is most favored for CH₃OH and TFE; the increase of proton donor strength makes the two *syn*-structures (*syn-1'* and *syn-1'a*) of either close or the same energy. The same trend can be seen in the AIM derived E_{cont} values, though the absolute numbers are somewhat lower than ΔE (ΔE_{ZPVE}) because only HH interaction is taken into account under the AIM approach. Dihydrogen bonding (*syn*-complexes) is clearly preferred over bonding to the metal (*anti-1'*); a similar trend was observed for $\text{Cp}^*\text{MH}(\text{dppe})$ analogues.^{3,5,42,43} These data are in agreement with the experimental evidence of DHB formation and explain why it is impossible to observe the hydrogen bonded *anti-1'* complex in the spectra.

Computational Study: Proton Transfer and Formation of *trans*-Dihydride. The most relevant to our study is the DFT/B3LYP study of proton transfer to the $\text{Cp}^*\text{FeH}(\text{dhpe})$ and $\text{CpFeH}(\text{dhpe})$ complexes ($\text{dhpe} = \text{H}_2\text{PCH}_2\text{CH}_2\text{PH}_2$) as models of $\text{Cp}^*\text{FeH}(\text{dppe})$ using either 1 or 2 molecules of HFIP or CF₃COOH are reported in ref 3. It has shown the clear preference of hydrogen bonding to the hydride ligand and its intermediacy in the formation of the $[\text{Fe}(\eta^2\text{-H}_2)]^+$ complex.³ Both theory and experiment have revealed no evidence for proton transfer to the metal in this case.^{2,3} Formation of *trans*- $[\text{Cp}^*\text{Fe}(\text{H})_2(\text{dppe})]^+$ has been shown to be intramolecular and occur via the “direct” pathway involving simultaneous H–H bond breaking and *cis*–*trans* isomerization. This pathway is slightly preferred over the “via Cp” pathway involving agostic C₅Me₅H intermediates.⁴ Its occurrence was strongly supported experimentally by KIE studies.⁴ Our calculations give the transition state for the “direct” transformation of $[\text{CpRu}(\eta^2\text{-H}_2)(\text{dppe})]^+$ (**2**) in *trans*- $[\text{CpRu}(\text{H})_2(\text{dppe})]^+$ (**3**) at 24.1 (ΔE^\ddagger) or 23.7 (ΔG^\ddagger) kcal·mol⁻¹, and the highest transition state for the “via Cp” pathway at 27.1 (ΔE^\ddagger), 28.5 (ΔG^\ddagger) kcal·mol⁻¹ (Supporting Information, Figure S6). These values

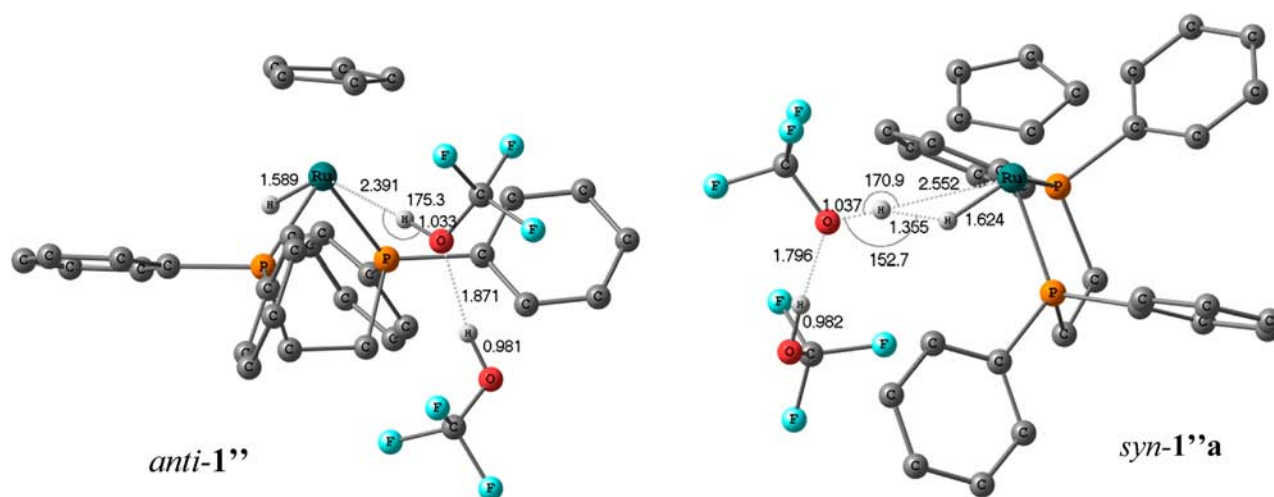


Figure 10. Optimized geometries of hydrogen bonded complexes of **1** with two CF_3OH molecules (syn-1''a and anti-1'') showing selected bond lengths (in Å) and angles (in degrees). Hydrogen atoms of Cp and dppe ligands are omitted for clarity.

are comparable to those calculated for $[\text{Cp}^*\text{MH}_2(\text{dppe})]^+$ cations ($M = \text{Fe}, \text{Os}$).^{4,42} However, these values are too high to support equilibrated $[\text{Ru}(\eta^2\text{-H}_2)]^+$ to $[\text{Ru}(\text{H})_2]^+$ transformation observed experimentally.

The energy profiles of proton transfer to $\text{CpRuH}(\text{dppe})$ were calculated using two CF_3OH molecules. The corresponding hydrogen bonded complexes (syn-1''a and anti-1'') were proven to be the reaction intermediates (Figure 10), which are connected with corresponding proton transfer products **2** and **3** via transition states TS-syn and TS-anti according to the IRC calculations. Interestingly the geometry of the dihydrogen bonded intermediate syn-1''a is closely related to that of syn-1'a complexes featuring same angles but shorter $\text{H}\cdots\text{H}(\text{O})$ and $\text{M}\cdots\text{H}(\text{O})$ distances in agreement with the higher proton donating strength of the CF_3OH dimer.

Proton transfer easily occurs in both hydrogen bonded complexes: the reaction transition states (TS-syn and TS-anti) are found less than $2.5 \text{ kcal}\cdot\text{mol}^{-1}$ above the corresponding hydrogen bonded minima (Figure 11). The proton transfer products—hydrogen bonded ion pairs $[\text{CpRu}(\text{H})_2(\text{dppe})]^+\cdots[\text{CF}_3\text{OHOCF}_3]^-$ and $[\text{CpRu}(\eta^2\text{-H}_2)(\text{dppe})]^+\cdots[\text{CF}_3\text{OHOCF}_3]^-$ (Supporting Information, Figure S5)—have comparable energies, the *trans*-dihydride **3** being 1.5

$\text{kcal}\cdot\text{mol}^{-1}$ more favorable on the free energy (ΔG_{gas}) scale. This energy difference is in agreement with the experimentally observed formation of a $2/3$ mixture. The positions of both transition states, TS-syn and TS-anti (Figure 11), are substantially lower than the TSs for the intramolecular isomerization of $[\text{CpRu}(\eta^2\text{-H}_2)(\text{dppe})]^+$ (**2**) to *trans*- $[\text{CpRu}(\text{H})_2(\text{dppe})]^+$ (**3**) along the “direct” or “via Cp” pathways (vide supra). Thus, the calculations show for the first time the preference of the intermolecular “deprotonation-reprotonation” pathway of $[\text{CpRu}(\eta^2\text{-H}_2)(\text{dppe})]^+$ (**2**) transformation to *trans*- $[\text{CpRu}(\text{H})_2(\text{dppe})]^+$ (**3**) where the deprotonation of **2** is the rate determining step. At that the transformation of DHB intermediate syn-1''a into hydrogen bonded anti-1'' does not require complete dissociation of syn-1''a ; the hydrogen bonded complex containing the alcohol molecules bonded simultaneously at *syn* and *anti* positions (syn-anti-1'' ; Figure 12) is a feasible reaction intermediate ($5.2 \text{ kcal}\cdot\text{mol}^{-1}$ above syn-1''a ; Figure 11).

Our experimental data show that the mechanism of $[\text{M}(\eta^2\text{-H}_2)]^+$ to $[\text{M}(\text{H})_2]^+$ transformation is different for semi-sandwich pentamethylcyclopentadienyl and cyclopentadienyl complexes of ruthenium. The irreversible first order reaction occurs in the case of $[\text{Cp}^*\text{MH}_2(\text{dppe})]^+$ complexes ($M = \text{Fe}, \text{Ru}, \text{Os}$),^{4,5,42} but it is reversible first order in the case of $[\text{CpRuH}_2(\text{dppe})]^+$. The DFT calculations performed suggest that it is the $[\text{Ru}(\eta^2\text{-H}_2)]^+$ deprotonation-reprotonation process what is responsible for *trans*- $[\text{Ru}(\text{H})_2]^+$ formation in case of $[\text{CpRuH}_2(\text{dppe})]^+$. Following this mechanism the energy profile can be drawn on the basis of experimental data (Figure 13). In the presence of alcohol excess the DHB complex (syn-1') should dominate at low temperatures, yielding the nonclassical cation **2** as the result of proton transfer. Following the computational results we believe that the activation parameters determined experimentally for $[\text{M}(\eta^2\text{-H}_2)]^+$ to $[\text{M}(\text{H})_2]^+$ transformation ($\Delta H^\ddagger = 16 \pm 1 \text{ kcal}\cdot\text{mol}^{-1}$, $\Delta S^\ddagger = -13 \pm 5 \text{ cal}\cdot\text{mol}^{-1}\cdot\text{K}^{-1}$) are those of the $[\text{M}(\eta^2\text{-H}_2)]^+$ deprotonation step. Under this assumption, the barrier for proton transfer to yield **2** from **1'** ($\Delta H_{\text{PT}}^\ddagger$) could be easily calculated as $10.8 \text{ kcal}\cdot\text{mol}^{-1}$. This value is too small to study the protonation kinetics by spectroscopic techniques at regular time scales. The temperature increase should allow formation of a hydrogen bond to the metal (anti-1'), which undergoes

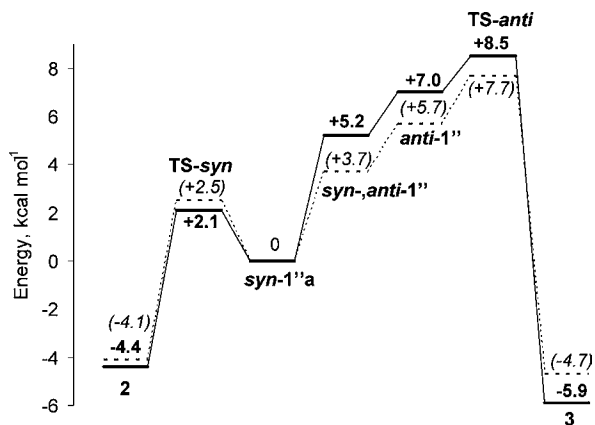


Figure 11. Electronic energy (ΔE , dashed line, italic numbers in parentheses) and free energy (ΔG , solid line, regular numbers) profiles for **1-2** CF_3OH system in gas phase.

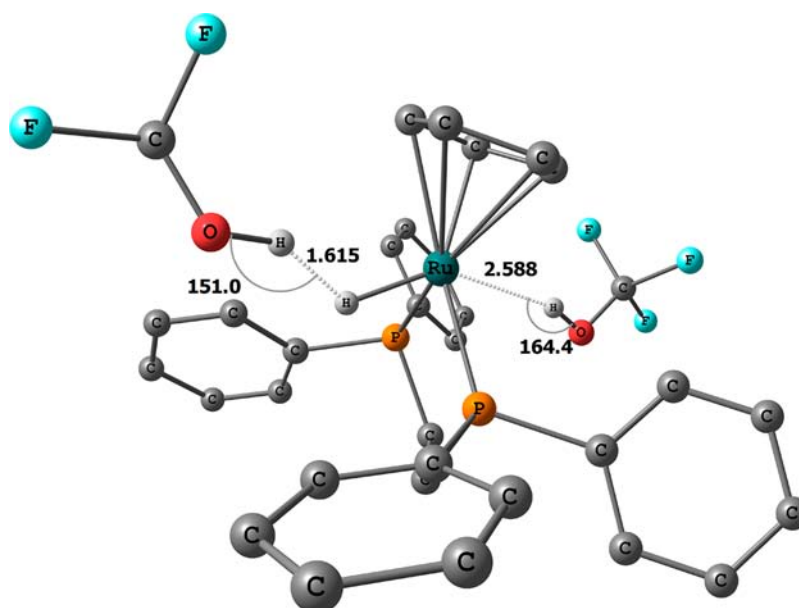


Figure 12. Optimized geometry of hydrogen bonded complex *syn-anti-1''* featuring simultaneous Ru...HO and RuH...HO bonds. Selected bond lengths (in Å) and angles (in degrees) are shown. Hydrogen atoms of Cp and dppe ligands are omitted for clarity.

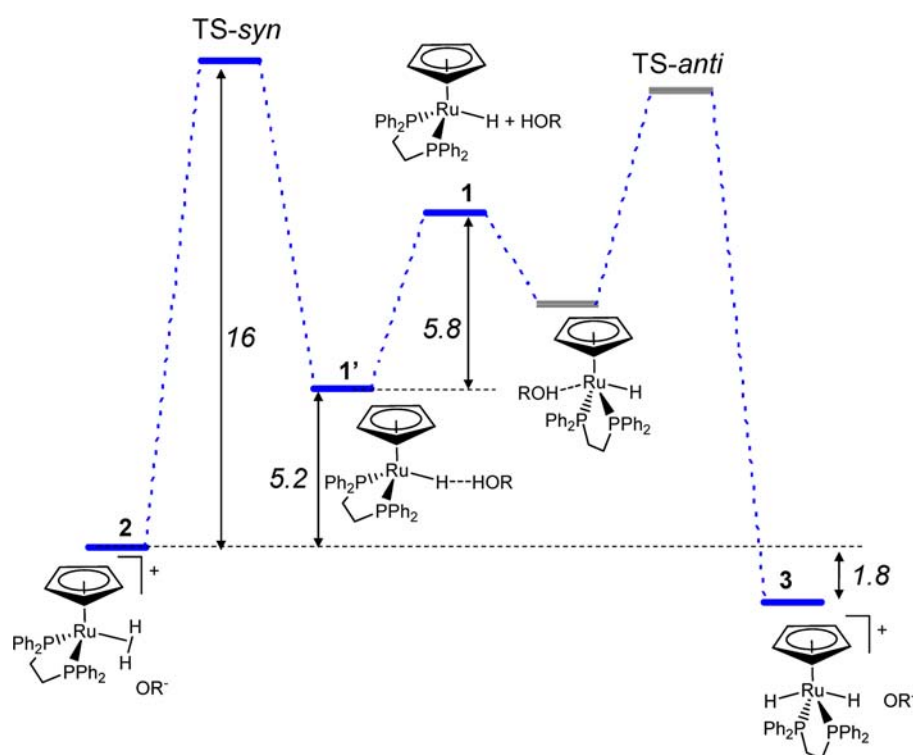


Figure 13. Enthalpy profile (ΔH , *italic numbers*, in kcal·mol⁻¹) for the reaction between **1** and HFIP based on the experimental data. Gray bars are drawn approximately since parameters of this step can not be observed experimentally.

proton transfer even more easy to yield the classical cation **3**. The driving force for the overall process is the thermodynamic favorability of the *trans*-dihydride **3**.

CONCLUSIONS

Our results show that substitution of Cp* by less bulky and less electron rich Cp in Cp'RuH(dppe) (Cp' = Cp or Cp*) still does not make it possible for hydrogen bonding to the metal in the presence of the hydride ligand. Variable temperature IR and

NMR spectroscopic data are consistent with dihydrogen bond formation, and two structures found computationally, when the proton donor is on the same side as the hydride ligand (*syn*), can be described as a dihydrogen bond with additional interaction to the metal. The ligand change lowers the hydride basicity, but it also diminishes the steric hindrance allowing better access of the proton donor to the metal in *anti* position. As the result the two proton accepting sites, hydride ligand and metal atom, become competitive, and direct proton transfer to

the metal to yield a *trans*-dihydride becomes operative in case of the Cp complex.

The low temperature (190–210 K) proton transfer leads via dihydrogen bonding to the nonclassical hydride $[\text{CpRu}(\eta^2\text{-H}_2)(\text{dppe})]^+$ (**2**) only. Upon the temperature increase (above 250–260 K) the latter transforms into classical dihydride *trans*- $[\text{CpRu}(\text{H})_2(\text{dppe})]^+$ (**3**) yielding a 1:2 mixture of **2** and **3**. According to both experiment and calculations the dihydrogen to dihydride isomerization mechanism involves deprotonation of dihydrogen complex to initial hydride with subsequent formation of $\text{Ru}\cdots\text{HA}$ hydrogen bond and proton transfer to the metal site. However being energetically less favorable, the hydrogen-bond to the metal atom ($\text{Ru}\cdots\text{HA}$) (*anti*-1') is still low populated and could not be observed experimentally. Evidences of such reaction mechanism are found for the first time, though the possibility of *anti*-proton transfer to the metal has been suggested for the formation of *trans*- $[\text{Cp}^*\text{Os}(\text{H})_2(\text{CO})_2]^+$ from $[\text{Cp}^*\text{Os}(\eta^2\text{-H}_2)(\text{CO})_2]^+$.⁴⁸ Thus, the metal-hydride dichotomy is a subject of modification of the ligand environment: change of steric and electronic properties upon substitution of Cp^* by Cp ring induces not only quantitative but very significant qualitative change in the hydride complex reactivity. The reversibility of *trans*- $[\text{CpRu}(\text{H})_2(\text{dppe})]^+$ formation is important for its operation as ionic hydrogenation catalyst,⁴⁹ so both $[\text{Ru}(\eta^2\text{-H}_2)]^+$ and $[\text{Ru}(\text{H})_2]^+$ can transfer proton to the product.

■ ASSOCIATED CONTENT

Supporting Information

Additional IR and NMR spectra, details of the AIM analysis, optimized geometries (Cartesian coordinates) of all the species. This material is available free of charge via the Internet at <http://pubs.acs.org>.

■ AUTHOR INFORMATION

Corresponding Author

*E-mail: nataliabelk@ineos.ac.ru (N.V.B.), shu@ineos.ac.ru (E.S.S.). Fax: +7 499 1355085 (N.V.B., E.S.S.).

Notes

The authors declare no competing financial interest.

■ ACKNOWLEDGMENTS

This work was supported by the Russian Foundation for Basic Research (projects 11-03-01210, 12-03-31326, 12-03-33018), the German-Russian Interdisciplinary Science Center (GRISC) funded by the German Federal Foreign Office via the German Academic Exchange Service (DAAD) (projects C-2010b-6 and C-2011a-4), and by the Division of Chemistry and Material Sciences of RAS.

■ REFERENCES

- Hamon, P.; Toupet, L.; Hamon, J.-R.; Lapinte, C. *Organometallics* **1992**, *11*, 1429–1431.
- Belkova, N. V.; Revin, P. O.; Epstein, L. M.; Vorontsov, E. V.; Bakhmutov, V. I.; Shubina, E. S.; Collange, E.; Poli, R. *J. Am. Chem. Soc.* **2003**, *125*, 11106–11115.
- Belkova, N. V.; Collange, E.; Dub, P.; Epstein, L. M.; Lemenovskii, D. A.; Lledós, A.; Maresca, O.; Maseras, F.; Poli, R.; Revin, P. O.; Shubina, E. S.; Vorontsov, E. V. *Chem.—Eur. J.* **2005**, *11*, 873–888.
- Baya, M.; Maresca, O.; Poli, R.; Coppel, Y.; Maseras, F.; Lledós, A.; Belkova, N. V.; Dub, P. A.; Epstein, L. M.; Shubina, E. S. *Inorg. Chem.* **2006**, *45*, 10248–10262.

- Belkova, N. V.; Dub, P. A.; Baya, M.; Houghton, J. *Inorg. Chim. Acta* **2007**, *360*, 149–162.
- Chinn, M. S.; Heinekey, D. M. *J. Am. Chem. Soc.* **1990**, *112*, 5166–5175.
- Chinn, M. S.; Heinekey, D. M. *J. Am. Chem. Soc.* **1987**, *109*, 5865–5867.
- Esteruelas, M. A.; Gomez, A. V.; Lahoz, F. J.; Lopez, A. M.; Onate, E.; Oro, L. A. *Organometallics* **1996**, *15*, 3423–3435.
- Jia, G.; Morris, R. H. *J. Am. Chem. Soc.* **1991**, *113*, 875–883.
- Conroy-Lewis, F. M.; Simpson, S. J. *J. Chem. Soc., Chem. Commun.* **1987**, 1675–1676.
- Jia, G.; Lough, A. J.; Morris, R. H. *Organometallics* **1992**, *11*, 161–171.
- Joslin, F. L.; Mague, J. T.; Roundhill, D. M. *Organometallics* **1991**, *10*, 521–524.
- Alonso, A. G.; Reventós, L. B. *J. Organomet. Chem.* **1988**, *338*, 249–254.
- Bruce, M. I.; Humphrey, M. G.; Swincer, A. G.; Wallis, R. C. *Aust. J. Chem.* **1984**, *37*, 1747–1755.
- Frisch, M. J.; Trucks, G. W.; Schlegel, H. B.; Scuseria, G. E.; Robb, M. A.; Cheeseman, J. R.; Montgomery, J. J. A.; Vreven, T.; Kudin, K. N.; Burant, J. C.; Millam, J. M.; Iyengar, S. S.; Tomasi, J.; Barone, V.; Mennucci, B.; Cossi, M.; Scalmani, G.; Rega, N.; Petersson, G. A.; Nakatsuji, H.; Hada, M.; Ehara, M.; Toyota, K.; Fukuda, R.; Hasegawa, J.; Ishida, M.; Nakajima, T.; Honda, Y.; Kitao, O.; Nakai, H.; Klene, M.; Li, X.; Knox, J. E.; Hratchian, H. P.; Cross, J. B.; Adamo, C.; Jaramillo, J.; Gomperts, R.; Stratmann, R. E.; Yazyev, O.; Austin, A. J.; Cammi, R.; Pomelli, C.; Ochterski, J. W.; Ayala, P. Y.; Morokuma, K.; Voth, G. A.; Salvador, P.; Dannenberg, J. J.; Zakrzewski, V. G.; Dapprich, S.; Daniels, A. D.; Strain, M. C.; Farkas, O.; Malick, D. K.; Rabuck, A. D.; Raghavachari, K.; Foresman, J. B.; Ortiz, J. V.; Cui, Q.; Baboul, A. G.; Clifford, S.; Cioslowski, J.; Stefanov, B. B.; Liu, G.; Liashenko, A.; Piskorz, P.; Komaromi, I.; Martin, R. L.; Fox, D. J.; Keith, T.; Al-Laham, M. A.; Peng, C. Y.; Nanayakkara, A.; Challacombe, M.; Gill, P. M. W.; Johnson, B.; Chen, W.; Wong, M. W.; Gonzalez, C.; Pople, J. A. *Gaussian 09*, Revision B.1; Gaussian, Inc.: Wallingford, CT, 2009.
- Perdew, J. P. In *Electronic Structure of Solids*; Ziesche, P., Eschrig, H., Eds.; Akademie Verlag: Berlin, Germany, 1991; p 11.
- Perdew, J. P. *Phys. Rev. B* **1986**, *33*, 8822–8824.
- Becke, A. D. *J. Chem. Phys.* **1993**, *98*, 5648–5652.
- Hay, P. J.; Wadt, W. R. *J. Chem. Phys.* **1985**, *82*, 270–283.
- Wadt, W. R.; Hay, P. J. *J. Chem. Phys.* **1985**, *82*, 284–298.
- Höllwarth, A.; Böhme, M.; Dapprich, S.; Ehlers, A.; Gobbi, A.; Jonas, V.; Köhler, K. F.; Stegmann, R.; Veldkamp, A.; Frenking, G. *Chem. Phys. Lett.* **1993**, *208*, 237–240.
- Hehre, W. J.; Ditchfield, R.; Pople, J. A. *J. Chem. Phys.* **1972**, *56*, 2257–2261.
- Hariharan, P.; Pople, J. A. *Theor. Chim. Acta* **1973**, *28*, 213–222.
- Fritsch, J.; Zundel, G. *J. Phys. Chem.* **1981**, *85*, 556–561.
- Wiberg, K. *Tetrahedron* **1968**, *24*, 1083–1096.
- Glendening, E. D.; Badenhop, J. K.; Reed, A. E.; Carpenter, J. E.; Bohman, J. A.; Morales, C.; Weinhold, F. *NBO*; Theoretical Chemistry Institute, University of Wisconsin: Madison, WI, 2001.
- Keith, T. A.; *AIMALL*, Version 11.09.18; TK Gristmill Software: Overland Park KS, 2011; <http://aim.tkgristmill.com>.
- Espinosa, E.; Alkorta, I.; Rozas, I.; Elguero, J.; Molins, E. *Chem. Phys. Lett.* **2001**, *336*, 457–461.
- Espinosa, E.; Molins, E.; Lecomte, C. *Chem. Phys. Lett.* **1998**, *285*, 170–173.
- Iogansen, A. V. *Theor. Experim. Khim.* **1971**, *7*, 302–311.
- Iogansen, A. V. *Spectrochim. Acta A* **1999**, *55*, 1585–1612.
- Epstein, L. M.; Belkova, N. V.; Shubina, E. S. In *Recent Advances in Hydride Chemistry*; Peruzzini, M., Poli, R., Eds.; Elsevier: Amsterdam, The Netherlands, 2001; pp 391–418.
- Belkova, N. V.; Besora, M.; Epstein, L. M.; Lledós, A.; Maseras, F.; Shubina, E. S. *J. Am. Chem. Soc.* **2003**, *125*, 7715–7725.
- Epstein, L. M.; Belkova, N. V.; Gutsul, E. I.; Shubina, E. S. *Pol. J. Chem.* **2003**, *77*, 1371–1383.

(35) Belkova, N. V.; Epstein, L. M.; Filippov, O. A.; Shubina, E. S. In *Spectroscopic Properties of Inorganic and Organometallic Compounds: Techniques, Materials and Applications*; Yarwood, J., Douthwaite, R., Duckett, S., Eds.; The Royal Society of Chemistry: Cambridge, U.K., 2012; Vol. 43, pp 1–28.

(36) Bakhmutov, V. I. *Dihydrogen bonds: Principles, Experiments and Applications*; John Wiley & Sons, Inc.: Hoboken, NJ, 2008.

(37) Belkova, N. V.; Shubina, E. S.; Epstein, L. M. *Acc. Chem. Res.* **2005**, *38*, 624–631.

(38) Bakhmutov, V. I.; Bakhmutova, E. V.; Belkova, N. V.; Bianchini, C.; Epstein, L. M.; Masi, D.; Peruzzini, M.; Shubina, E. S.; Vorontsov, E. V.; Zanolini, F. *Can. J. Chem.* **2001**, *79*, 479–489.

(39) Belkova, N. V.; Epstein, L. M.; Shubina, E. S. *Eur. J. Inorg. Chem.* **2010**, *2010*, 3555–3565.

(40) Dub, P. A.; Baya, M.; Houghton, J.; Belkova, N. V.; Daran, J. C.; Poli, R.; Epstein, L. M.; Shubina, E. S. *Eur. J. Inorg. Chem.* **2007**, 2813–2826.

(41) Belkova, N. V.; Epstein, L. M.; Shubina, E. S. *Eur. J. Inorg. Chem.* **2010**, 3555–3565.

(42) Dub, P. A.; Belkova, N. V.; Filippov, O. A.; Silantyev, G. A.; Daran, J.-C.; Epstein, L. M.; Poli, R.; Shubina, E. S. *Eur. J. Inorg. Chem.* **2010**, 1489–1500.

(43) Filippov, O. A.; Belkova, N. V.; Epstein, L. M.; Lledós, A.; Shubina, E. S. *ChemPhysChem* **2012**, *13*, 2677–2687.

(44) Popelier, P. L. A. *J. Phys. Chem. A* **1998**, *102*, 1873–1878.

(45) Grabowski, S. J. *J. Phys. Chem. A* **2001**, *105*, 10739–10746.

(46) Rozas, I. *Phys. Chem. Chem. Phys.* **2007**, *9*, 2782–2790.

(47) Poater, J.; Fradera, X.; Sola, M.; Duran, M.; Simon, S. *Chem. Phys. Lett.* **2003**, *369*, 248–255.

(48) Egbert, J. D.; Bullock, R. M.; Heinekey, D. M. *Organometallics* **2007**, *26*, 2291–2295.

(49) Guan, H.; Iimura, M.; Magee, M. P.; Norton, J. R.; Zhu, G. J. *Am. Chem. Soc.* **2005**, *127*, 7805–7814.